Journal of Materials Chemistry B

RSC Publishing

PAPER

View Article Online
View Journal | View Issue

Cite this: *J. Mater. Chem. B*, 2013, **1**, 676

Biotin-decorated fluorescent silica nanoparticles with aggregation-induced emission characteristics: fabrication, cytotoxicity and biological applications†

Min Li,[ab] Jacky W. Y. Lam,[b] Faisal Mahtab,[b] Sijie Chen,[b] Weijie Zhang,[a] Yuning Hong,[b] Jun Xiong,[a] Qichang Zheng*[a] and Ben Zhong Tang*[b]

Received 22nd September 2012
Accepted 15th November 2012

DOI: 10.1039/c2tb00155a

www.rsc.org/MaterialsB

Biotin-decorated fluorescent silica nanoparticles (FSNPs) were successfully fabricated by a sol–gel reaction of silole-functionalized siloxane followed by a sequential reaction with tetraethoxysilane, (3-aminopropyl) triethoxysilane and biotin. The FSNPs were uniformly sized, spherical in shape and monodispersed. While their silole precursor was non-emissive in solution, the suspension of the FSNPs emitted strong green light upon photoexcitation due to the aggregation-induced emission characteristics of the silole aggregates in the hybrid nanoparticles. Morphology study and cell viability, trypan blue exclusion, Annexin V-FITC/PI apoptosis and ROS generation assays showed that the FSNPs showed low toxicity to living cells. The FSNPs worked as fluorescent visualizers for selective imaging of the cytoplasm of tumor cells with over-expressed biotin receptors. The fluorescent nanoparticles were lastingly retained inside the living cells, thus enabling long-term tumor cell tracking over multiple passages and quantitative analysis of tumor cell migration.

Introduction

Fluorescent silica nanoparticles (FSNPs) are promising materials for bioanalysis and bioimaging as well as for disease diagnosis and therapy because of their characteristic features including biocompatibility, inertness, hydrophilicity, size tuning, ease of surface modification, *etc.*[1] Since hundreds of fluorescent molecules are encapsulated in a single nanoparticle, the detection sensitivity of FSNPs is much higher than that of direct fluorophore labeling. To date, FSNPs have been used widely in DNA microarrays,[2] immunofluorescence technique,[3] analogue luminescence detection,[4] tissue imaging,[5] cell imaging[6] and especially tumor cell imaging.[1b,5,7] As silica nanoparticles have been found to exhibit no remarkably toxic effect on living cells,[8] they thus possess the potential prospect in tumor cell imaging for early diagnosis and cell tracking.

Conventional dyes have been used for the fabrication of FSNPs.[9] These fluorophores emit strongly in solutions but become weakly emissive or non-luminescent in the solid state due to the strong π–π stacking interactions, which promote the formation of detrimental species such as excimers or exciplexes.[10] The weak emission offered by the FSNPs has resulted in poor sensitivity in fluorescence sensory systems, especially in bioassays of trace amounts of biomolecules. The sensitivity cannot be enhanced by using higher fluorophore concentrations due to the aggregation-caused quenching (ACQ) effect. The development of inorganic quantum dots can surmount these disadvantages but create new problems such as difficult synthesis, limited variety and high cytotoxicity.[11]

We observed a novel phenomenon of aggregation-induced emission (AIE) that is exactly opposite to the ACQ effect in a series of propeller-like molecules. Instead of quenching, aggregate formation has boosted their fluorescence quantum yields by more than 300-fold, turning them from weak fluorophores in the solution state to strong emitters in the solid state.[10,12] The restriction of intramolecular rotation in the aggregated state has been proposed as the main cause for the AIE effect.[10,13] Because of their efficient solid-state emission, AIE luminogens are thus ideal fluorophores for the fabrication of FSNPs. In our previous work, we succeeded in creating FSNPs hybridized with AIE luminogens by a one-step surfactant free sol–gel process. These highly emissive FSNPs pose good colloidally stability and are non-toxic to living cells, thus making them promising fluorescent visualizers for intracellular imaging.[14] By modifying the fabrication procedure, silica nanoparticles with both strong light emission and high magnetization are prepared, which can function as selective cell

[a]*Department of Hepatobiliary Surgery, Union Hospital, Tongji Medical College, Huazhong University of Science and Technology, Wuhan 430022, China. E-mail: qc_zheng@mail.hust.edu.cn; Fax: +86-27-8535-1676; Tel: +86-27-8535-1623*

[b]*Department of Chemistry, Institute for Advanced Study, State Key Laboratory of Molecular Neuroscience, Institute of Molecular Functional Materials and Division of Biomedical Engineering, The Hong Kong University of Science and Technology, Clear Water Bay, Kowloon, Hong Kong, China. E-mail: tangbenz@ust.hk; Fax: +852-2358-1594; Tel: +852-2358-7375*

† Electronic supplementary information (ESI) available: IR spectra, SEM images, TGA thermograms, fluorescent photographs, HE staining, TEM images, XPS and EDX patterns. See DOI: 10.1039/c2tb00155a

imaging bioprobes and immobilize bovine serum albumin efficiently.[15]

To widen the applicability of the AIE-loaded silica nanoparticles, their selectivity should be further improved. It is known that conjugation of targeting ligands such as proteins, peptides and aptamers on the surface of nanoparticles can enhance their binding affinity and facilitate receptor-mediated internalization,[16] thus enabling selective targeting and efficient intracellular uptake. Biotin (vitamin B7 or vitamin H), a member of the vitamin family for growth promotion at the cellular level, is one of the most common tumor recognition moieties because tumor cells require extra biotin to sustain their rapid growth and compared to the normal cells, biotin-specific receptors are thus generally over-expressed on their surface.[17] Thus, biotin has attracted particular interest in cancer-targeting drug carrier and fluorescent nanoparticles for specific tumor cell targeting. For example, Panyam and colleagues prepared a biotin-functionalized drug delivery carrier, which significantly improved the therapeutic efficacy of tumors.[18] Kwon also modified gold nanoparticles with biotin and rhodamine B to interact selectively with cancer cells for diagnosis and therapy.[17d] However, examples of AIE-active silica nanoparticles functionalized with biotin have not been described.

In this paper, we aim to synthesize such nanoparticles for specific living tumor cell imaging. A series of experiments had been carried out to evaluate the toxicity or biocompatibility of the synthesized nanoparticles. The biotin-decorated FSNPs emitted strong photoluminescence (PL) under UV excitation and interacted selectively with tumor cells with over-expressed biotin receptors and internalized into cytoplasmic regions. They can stay inside the live cells for long periods of time, thus enabling long term cell tracing over multiple passages as well as analysis of tumor cell migration quantitatively.

Results and discussion

Fabrication of biotin-decorated FSNPs

With a view to fabricate FSNPs with strong light emissions in the solid state and biotin moieties on the surface for specific cancer cell targeting, we synthesized a silole-containing siloxane (**1**) by stirring a dimethylsulfoxide (DMSO) solution of **2** and (3-aminopropyl)triethoxysilane (APS) at room temperature for 24 h (Scheme 1). The sol–gel reaction of **1** followed by reaction with tetraethoxysilane afforded FSNP-**1** with a core–shell structure.[14,15] Addition of APS into the reaction mixture generated FSNP-**1**-NH_2 with numerous amino groups decorated on the surface, enabling it to undergo amidation reaction with biotin in the presence of 1,3-dicyclohexylcarbodiimide (DCC) and 4-(dimethylamino)pyridine (DMAP) to furnish FSNP-**1**-biotin.

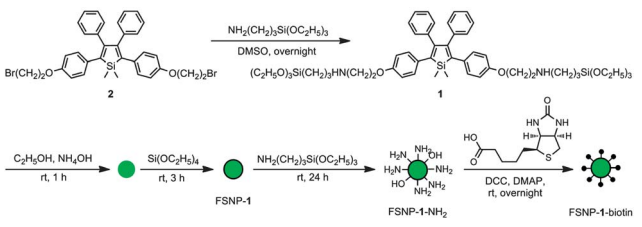

Scheme 1 Fabrication of biotin-decorated fluorescent silica nanoparticles.

Structural characterization

We first characterized FSNP-**1**-biotin by IR spectroscopy. The IR spectrum of FSNP-**1**-biotin is given in Fig. S1 in the ESI;† for comparison; the spectra of FSNP-**1**-NH_2 and biotin are also provided in the same figure. The Si–OH, Si–O and N–H stretching vibrations of FSNP-**1**-NH_2 occurred at 951, 1707 and 3321 cm^{-1}, respectively. After biotin modification, the absorption at 3321 cm^{-1} was enhanced and new peaks associated with C=O stretching vibrations emerged at 1638 and 1707 cm^{-1} in FSNP-**1**-biotin, revealing that biotin was covalently grafted on the surface of FSNP-**1**-NH_2 through amidation reaction. Analysis by transmission electron microscopy (TEM) showed that both FSNP-**1**-NH_2 and FSNP-**1**-biotin were spherical in shape and uniform in diameters with narrow size distributions (Fig. 1). Compared to FSNP-**1**-NH_2, FSNP-**1**-biotin possessed a much rougher surface. The average particle size of FSNP-**1**-NH_2 was measured to be 48.19 ± 2.82 nm, while that of FSNP-**1**-biotin was slightly larger (50.50 ± 2.91 nm). Similarly, the images from a scanning electron microscope (SEM) given in Fig. S2† showed that the surface morphology of FSNP-**1**-NH_2 altered little after the biotin conjugation. To realize the composition of the nanoparticles, X-ray photoelectron spectroscopy (XPS) and energy dispersive X-ray spectroscopy (EDX) were carried out and the results are summarized in Table S1.† XPS analyses revealed no sulfur atom on the surface of FSNP-**1**-NH_2, while a trace amount of sulfur element (0.3%) was detected in FSNP-**1**-biotin. Similar results were also obtained from the EDX analysis, proving that biotin is successfully conjugated on the surface of FSNP-**1**-NH_2. The thermal stability of the FSNPs was investigated by thermogravimetric analysis (TGA). As shown in Fig. S3,† FSNP-**1**-NH_2 possessed high thermal stability and started to degrade at a temperature of ~300 °C. Even when heated up to 800 °C, more than 70% of its

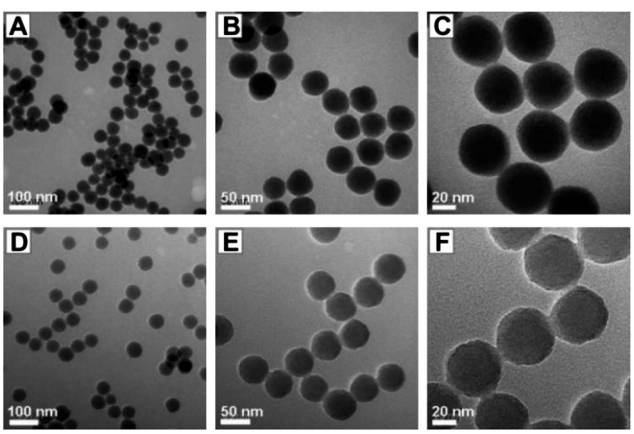

Fig. 1 TEM images of (A–C) FSNP-**1**-NH_2 and (D–F) FSNP-**1**-biotin at different magnifications.

weight was retained. FSNP-**1**-biotin was also thermally quite stable and degraded at a similar temperature with high residual yield at 800 °C. Since biotin decomposed completely at 650 °C, the amount of biotin grafted on FSNP-**1**-biotin could be calculated as the weight difference between the thermograms of FSNP-**1**-NH_2 and FSNP-**1**-biotin at this temperature and was equal to 6.92 wt%.

Light emission

The PL spectra of a solution of **1** and suspensions of FSNP-**1**-NH_2 and FSNP-**1**-biotin in ethanol are displayed in Fig. 2. Nearly no fluorescence signals were recorded when the ethanol solution of **1** was photoexcited. In the solution state, the multiple peripheral phenyl rings in the isolated molecules of **1** undergo active intramolecular rotation, which effectively annihilates their excited states and hence renders the luminogen non-emissive.[10] When the molecules of **1** are covalently incorporated into and aggregate in the silica networks of FSNP-**1**-NH_2 and FSNP-**1**-biotin, strong PL spectra peaked at ~490 nm are recorded. Evidently, **1**, similar to its congener **2**, is AIE-active. The rigid silica network largely restricts the intramolecular rotations of the luminogen. This blocks the nonradiative relaxation channels and populates the radiative excitons,[10,12a,19] thus making the FSNPs highly luminescent. Under the same measurement conditions, the PL intensities of FSNP-**1**-NH_2 and FSNP-**1**-biotin were 95- and 87-folds higher than that of **1** in an ethanol solution, respectively. The photographs of a solution of **1** and the suspensions of FSNP-**1**-NH_2 and FSNP-**1**-biotin taken under UV exposure from a hand-held UV lamp are shown as an inset in Fig. 2. While intense light was emitted from FSNP-**1**-NH_2 and FSNP-**1**-biotin, the solution of **1** was invisible under the UV illumination. This visual observation further substantiates that the intramolecular rotation of **1** is restricted by its covalent melding with the silica matrix. The light emission was very stable, with no detectable change in the PL spectrum after FSNP-**1**-biotin was put on shelves for 6 months without protecting from light and air (Fig. S4†).

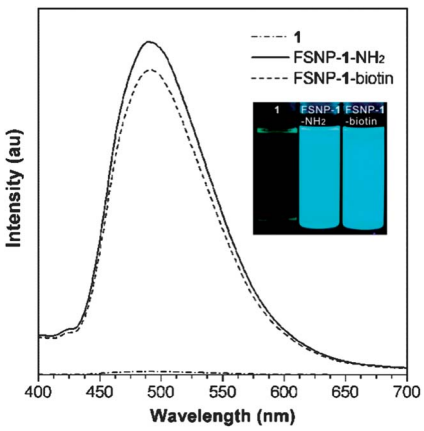

Fig. 2 PL spectra of **1**, FSNP-**1**-NH_2 and FSNP-**1**-biotin in ethanol solutions. Nanoparticle concentration: 200 μg mL^{-1}; excitation wavelength: 370 nm. Inset: photographs of ethanol solutions of **1**, FSNP-**1**-NH_2 and FSNP-**1**-biotin taken under 365 nm UV irradiation from a hand-held UV lamp.

Cytotoxicity

To find useful biological applications, a luminogen should neither inhibit nor promote the growth of living cells. To evaluate the toxicity of FSNP-**1**-biotin, we first studied the morphology change of HeLa and mouse fibroblast NIH 3T3 cells cultured in the presence of FSNP-**1**-biotin. As shown in Fig. S5,† only a small amount of cells showed vacuole shrinkage and chromatin condensation, suggesting that FSNP-**1**-biotin possessed good biocompatibility. A cell viability assay was also carried out at nanoparticle concentrations of 0.1, 1, 10, 100 and 200 μg mL^{-1} for 48 h using a WST-8 cell counting kit. The cell viability decreased with an increase in the nanoparticle concentration. Compared with the control group, the nanoparticles had no discernible deleterious effects on the viability of both HeLa and 3T3 cells ($P > 0.05$) at concentrations below 100 μg mL^{-1} (Fig. 3A). At 100 μg mL^{-1}, the viability decreased to 81.60% and 85.55% for HeLa cells and 3T3 cells ($P < 0.05$), respectively. To further verify the cytotoxicity of FSNP-**1**-biotin, the cell survival was examined by the trypan blue exclusion assay.[8a] The viable cells exclude the trypan blue dye and are not stained to identify living cells. At a nanoparticle concentration of 100 μg mL^{-1}, the cell survival of HeLa cells and 3T3 cells was reduced to 88.49% and 86.74% ($P < 0.05$), respectively, which echoed in the foregoing data (Fig. 3B). Consequently, the cells were exposed to up to 80 μg mL^{-1} of FSNP-**1**-biotin for the experiments afterward in accordance with the preliminary cytotoxicity effect and requisite nanoparticle concentration for tumor cell imaging.

Cell apoptosis is an important parameter for the toxicity of nanomaterials. Nanoparticles could induce apoptosis through

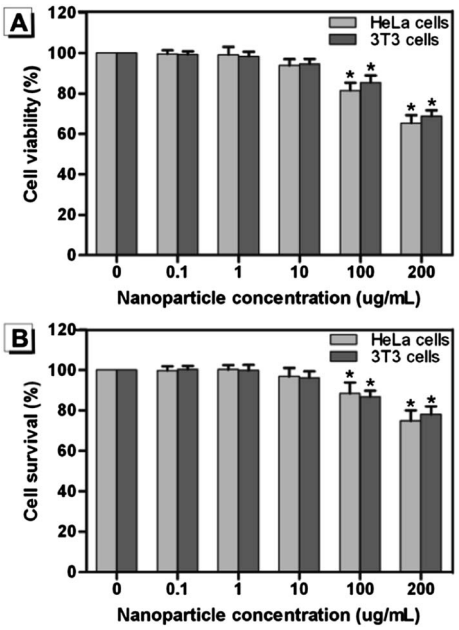

Fig. 3 Cytotoxicity of FSNP-**1**-biotin on HeLa and 3T3 cells evaluated by (A) CCK 8 and (B) trypan blue exclusion assays. The data were analyzed by one-way analysis of variance followed by Dunnett's test and the mean value ± standard deviation was reported. * Means $P < 0.05$ when compared with the control (0 μg mL^{-1}) and indicates an obvious toxicity.

many kinds of pathways. The apoptotis-related proteins, such as Bcl-2, Bax, CytC and Caspase-3, were up-regulated when HepG2 cells were exposed to silica nanoparticles.[20] Herein, the quantification of apoptosis of HeLa and 3T3 cells was studied by flow cytometry (FCM) with Annexin V-FITC/propidium iodide (PI) double staining assay at different concentrations of FSNP-**1**-biotin. The cells stained with Annexin V-FITC alone represent early apoptosis, while those labelled with PI demonstrate necrosis. The late apoptotic cells are stained with both fluorescent dyes. As depicted in Fig. 4, FSNP-**1**-biotin could induce apoptosis in a dose-dependent manner. Compared with the control group, the number of apoptotic cells increased with increasing nanoparticle concentration. In the presence of 80 μg mL^{-1} of nanoparticles, obvious apoptosis was observed in both HeLa and 3T3 cells ($P < 0.05$).

The oxidative stress-mediated pathway is demonstrated as one of the apoptotic mechanisms due to the induction of nanomaterials.[21] Nanoparticles can induce production of intracellular reactive oxygen species (ROS), which can change the permeability of a mitochondrial membrane, damage the ultrastructure of mitochondria[21a] and then trigger secondary damage effects such as mitochondrial dysfunction and DNA damage.[22] The ROS assay was based on the peroxide-dependent oxidation of DCFH-DA to form a fluorescent compound named dichlorofluorescein. Herein, the HeLa and 3T3 cells were treated with various concentrations of FSNP-**1**-biotin for 24 h. Afterwards, they were washed with a buffer solution and incubated with DCFH-DA for 20 min. The fluorescence from the cells was then immediately measured by a FCM. The ROS generation and hence the fluorescence from the solution became higher when HeLa and 3T3 cells were cultured with an increasing amount of FSNP-**1**-biotin nanoparticles (Fig. 5). The difference in the ROS generation between the control and treated cells was small at a nanoparticle concentration of 40 μg mL^{-1} but was obvious at 80 μg mL^{-1} (Fig. 5C). However, when compared to the positive (Rosup) control, the extent of ROS generation was not large at such nanoparticle concentrations. On the other hand, the intuitive fluorescent images shown in Fig. 5D also

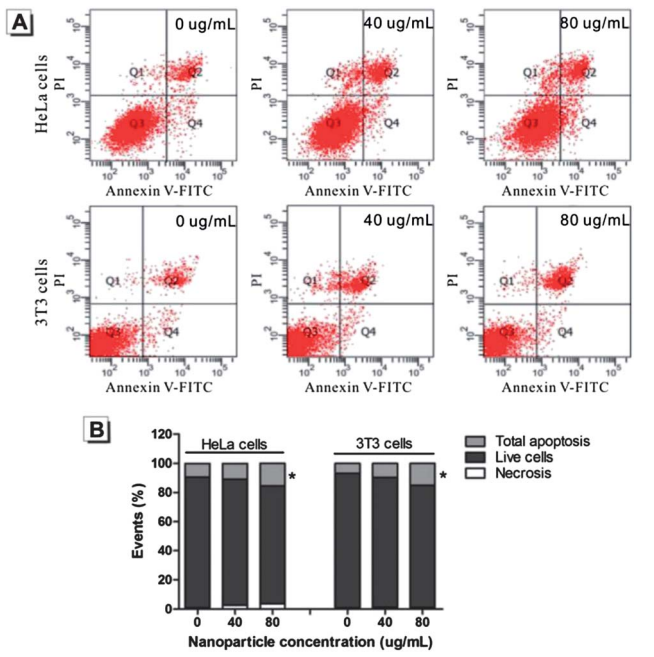

Fig. 4 Apoptosis of HeLa and 3T3 cells in the presence of FSNP-**1**-biotin for 48 h. The cytograms given in (A) showed the fluorescence from the cells measured using the Annexin V-FITC/PI assay at different nanoparticle concentrations. According to the emission intensity from the fluorescence dye ("+" = high, "−" = low), four regions, named Q1 (Annexin V-FITC −, PI +), Q2 (Annexin V-FITC +, PI +), Q3 (Annexin V-FITC −, PI −) and Q4 (Annexin V-FITC +, PI −) were divided, which represented the necrotic, late apoptotic, living and early apoptotic cells, respectively. (B) Quantitative analysis of cell apoptosis from three independent experiments. The total apoptotic cells (Q2 + Q4) were shown in the histograms, analyzed by Dunnett's test and compared with the control (0 μg mL^{-1}). * Means $P < 0.05$ and indicates that the total number of apoptotic cells is significantly different from that of control.

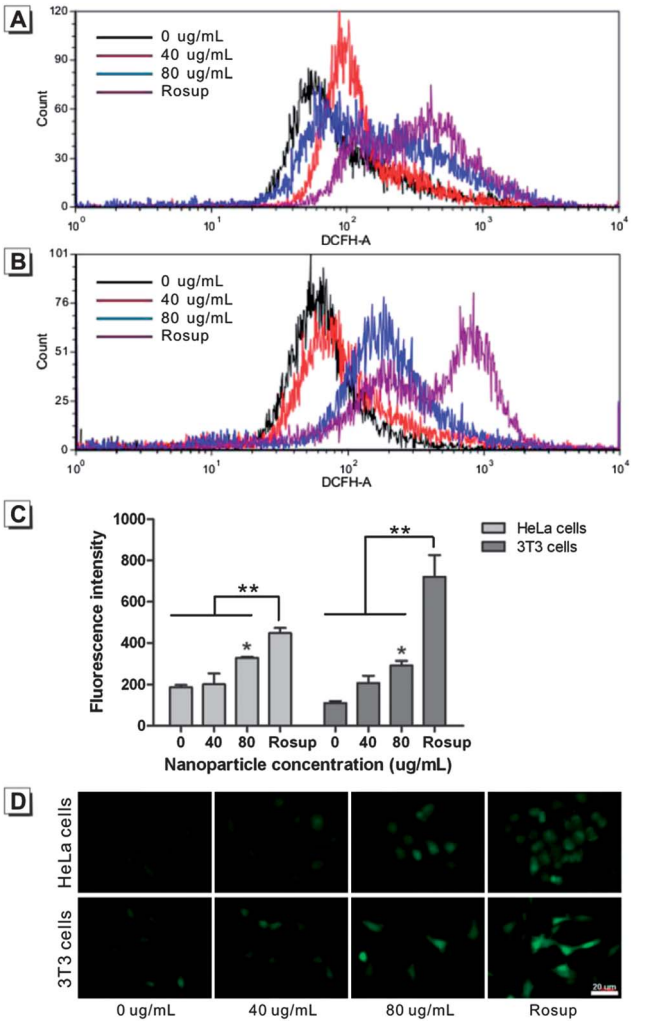

Fig. 5 Intracellular ROS generation of HeLa and 3T3 cells in the presence of FSNP-**1**-biotin analyzed by the DCFH-A assay for 24 h. (A and B) FCM histograms of HeLa and 3T3 cells, respectively, in the absence and presence of different nanoparticle concentrations. (C) The data were analyzed by one-way analysis of variance followed by Dunnett's test, compared with a negative (0 μg mL^{-1}) or positive (Rosup) control and reported as mean value ± standard deviation. * Means $P < 0.05$ when compared with the negative control. ** Means $P < 0.05$ when compared with the positive control. (D) Fluorescent images of HeLa and 3T3 cells associated with ROS generation in the absence and presence of FSNP-**1**-biotin.

indicated that the nanoparticles induced ROS generation when the cells were exposed to a high concentration of FSNP-**1**-biotin.

Tumor cell targeting and long-term cell tracking

In our previous study, we found that FSNPs hybridized with AIE luminogens can be utilized as fluorescent visualizers for intracellular imaging.[14] Would FSNP-**1**-biotin show similar or even better performance? To test this, the targeting property of FSNP-**1**-biotin was investigated using HeLa and BEL-7402 cells, which are typical cell lines for cervical carcinoma and hepatocellular carcinoma, respectively, with over-expressed biotin receptors. Normal liver cells LO2 containing less-expressed receptors were also used in the investigation for the purpose of comparison. After 3 h staining, strong PL was emitted from the HeLa and BEL-7402 cells, while dim fluorescence was observed from LO2 cells (Fig. 6). This phenomenon should be attributed to receptor-mediated endocytosis.[23] For tumor cells with over-expressed biotin receptors on the surface, FSNP-**1**-biotin binds the cell membrane *via* ligand–receptor interaction (Scheme 2). The interaction of the nanoparticles with the biotin receptor triggers cell internalization into intracytoplasmic vesicles or the formation of clathrin-coated vesicles. The nanoparticles may be further processed in vacuoles and endosomes, which are then eventually released to the cytoplasm. On the other hand, the nanoparticles without biotin coating enter the cells mainly by caveolae-dependent endocytosis, whose rate, specificity and affinity are much lower than those of clathrin-dependent endocytosis.[23] The uptake of FSNP-**1**-biotin nanoparticles by LO2 cells is low due to the absence of biotin receptors on their surface. Moreover, they, unlike HeLa and BEL-7402 cells, require a small amount of biotin for proliferation, thus resulting in low nanoparticle uptake and weak fluorescence.

To prove the existence of ligand–receptor interactions or the occurrence of receptor-mediated endocytosis, fluorescence imaging of tumor cells by FSNP-**1**-biotin was carried out in the presence of free biotin. As shown by the images given in Fig. 7, the fluorescence from the HeLa and BEL-7402 cells was markedly decreased when they were pretreated with a 10 μg mL^{-1} biotin solution prior to staining. This result suggests that the free biotin molecules competitively bind to the biotin receptors on the surface of tumor cells and interdict the receptor-mediated endocytosis of FSNP-**1**-biotin. Evidently, bio-conjugation of FSNP-**1**-NH_2 with biotin molecules has enhanced the targeting efficiency and endocytosis of the resulting FSNP-**1**-biotin.

The uptake of nanoparticles by cells involves several different pathways such as nonspecific diffusion, phagocytosis and receptor-mediated or fluid phase endocytosis.[24] To confirm the uptake and distribution of FSNP-**1**-biotin, we analyzed the HeLa cells treated with FSNP-**1**-biotin for 12 h by TEM. The nanoparticles were distinguished based on their diameters and spherical shape. As displayed in Fig. S6,† the nanoparticles were

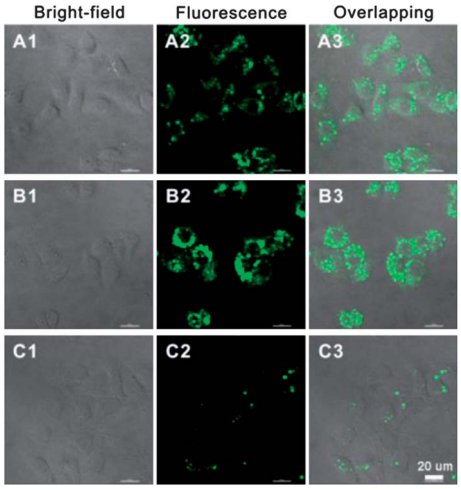

Fig. 6 Bright-field, fluorescence and overlapping images of (A1–A3) HeLa, (B1–B3) BEL-7402 and (C1–C3) LO2 cells stained with FSNP-**1**-biotin for 3 h.

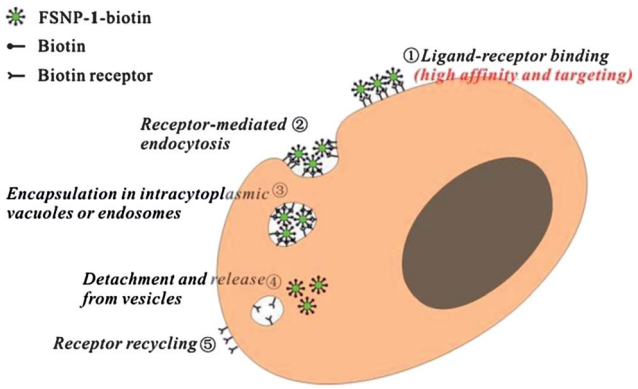

Scheme 2 Schematic illustration of tumor cell targeting and imaging by FSNP-**1**-biotin.

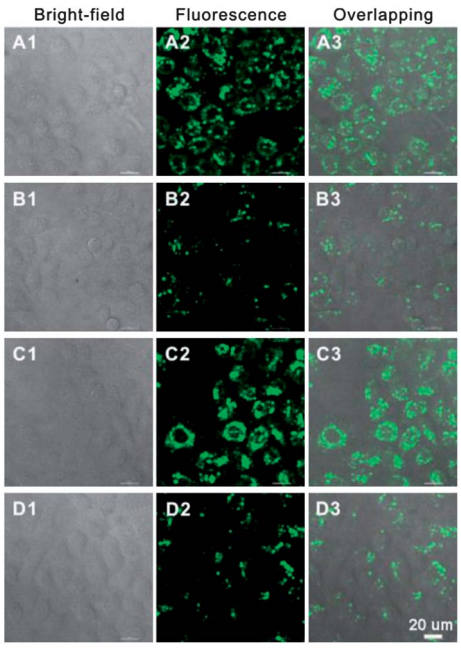

Fig. 7 Bright-field, fluorescence and overlapping images of (A and B) HeLa and (C and D) BEL-7402 cells stained with FSNP-**1**-biotin in the (A and C) absence and (B and D) presence of free biotin.

internalized into cells *via* receptor-mediated endocytosis just as depicted in Scheme 2. This facilitates their uptake and internalization in the cells (Fig. S6A†). The nanoparticles were then released into the cytoplasm (Fig. S6B†) and distributed as isolated species or clusters (Fig. S6C†). No nanoparticles were found in the nucleus, which is consistent with the literature results, and it was presumably due to the large size of the nanoparticles.[25]

In our previous work, we found that a cytophilic fluorescent bioprobe fabricated from 1-decyl-1-methyl-2,5-bis{4-[(*N*,*N*-diethylamino)methyl]phenyl}-3,4-diphenylsilole could track living cells for four passages, while almost no PL signals were detected in cells labelled with MitoTracker Green FM, a commercial dye, after two generations.[26] As an excellent tumor targeting probe, FSNP-**1**-biotin should also possess the property of high photostability and long-term tracking. Thus, the fluorescence from the HeLa and BEL-7402 cells stained with FSNP-**1**-biotin was investigated in a continuous manner of cell culture. The tumor cells were observed after incubation with 40 μg mL^{-1} nanoparticles for 24 h. When 70–80% confluence was reached, the cells were trypsinized, counted and subcultured at a density of 2×10^5 cells per well into a 6-well plate. Generally, the cells grow into another generation within 1 day. Although the PL from the cells became weaker along the passage due to the division of the nanoparticles accompanied by cellular fission, they were still visible even after 5 day culture (Fig. 8). Evidently, FSNP-**1**-biotin is a superb long-term cell tracer. No fluorescence was observed in the cell nucleus, which was consistent with the TEM analysis. We prolonged the culture to 7 days. Although dim fluorescence was still observed from the cells, their morphology was hard to be discernible (Fig. S7†). Thus, the retention time of the nanoparticles inside the cell is approximately one week.

Tumor cell migration

Cell migration is an important pathological process in tumor cells and reflects their ability of tissue invasiveness and metastasis.[27] In the above discussion, we found that FSNP-**1**-biotin could selectively stain tumor cells with over-expressed biotin receptors and enable long-term cell tracing over multiple passages. With such regard, we explored the possibility of using FSNP-**1**-biotin to track the migration of tumor cells. Briefly, different concentrations of serum were loaded to the medium in the lower compartment. FSNP-**1**-biotin labelled HeLa cells were then introduced into the upper compartment of a cell. Because the HeLa cells require additional nutrients to maintain their rapid proliferation, they are thus induced to move from the upper compartment to the lower one. The migrated cells were collected by trypsin and the fluorescence of the cell suspension was then measured. As shown in Fig. 9A, the fluorescence became stronger with an increase in the serum concentration. Since the PL intensity is associated with the number of labelled cells, this makes quantitative analysis possible. Same result was achieved by the conventional crystal violet staining method (Fig. 9B) but the fluorescence-based technique was more objective and accurate.

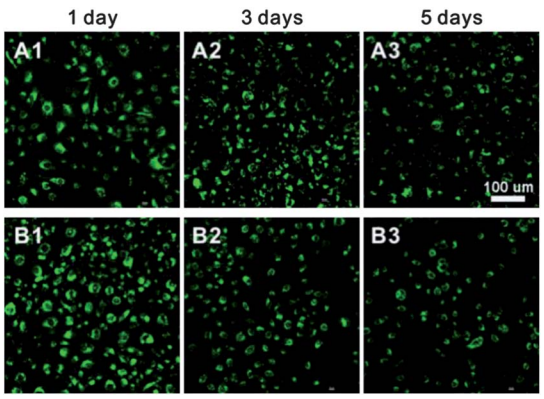

Fig. 8 Fluorescent images of (A1–A3) HeLa and (B1–B3) BEL-7402 cells stained with FSNP-**1**-biotin at different times.

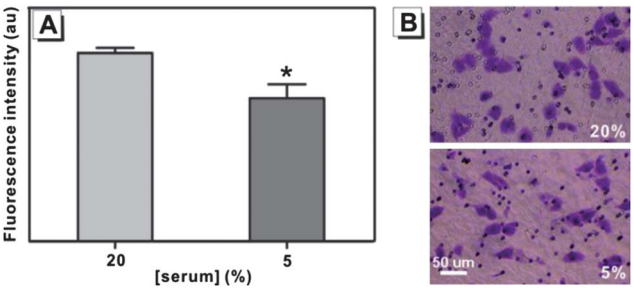

Fig. 9 Migration of FSNP-**1**-biotin-labeled HeLa cells treated with 20 or 5% serum for 24 h. (A) Quantitative analysis of cell migration at different serum concentrations using HeLa cells labeled with FSNP-**1**-biotin. The data are expressed as mean value ± standard deviation from three independent experiments. * Means $P < 0.05$ and indicates significant difference when compared to cells treated with 20% serum. (B) Optical images of migrated HeLa cells stained by the conventional crystal violet.

Conclusions

In summary, biotin-decorated fluorescent silica nanoparticles were successfully fabricated by a surfactant-free sol–gel reaction of silole-functionalized siloxane followed by esterification reaction with biotin. The structure of FSNP-**1**-biotin was investigated by IR, TEM, SEM and XPS analyses. The FSNP-**1**-biotin was uniformly sized, spherical in shape and monodispersed. Although their silole precursor was non-emissive, the FSNP-**1**-biotin emitted strong green light upon photoexcitation, as a result of the aggregation-induced emission characteristics of the silole aggregates in the hybrid nanoparticles. Morphology study and cell viability, trypan blue exclusion, Annexin V-FITC/PI apoptosis and ROS generation assays showed that FSNP-**1**-biotin possessed low toxicity to living cells. The FSNP-**1**-biotin can be utilized to selectively image the cytoplasm of tumor cells with over-expressed biotin receptors. They can stay inside the living cells for a long period of time, thus enabling long term tumor cell tracing over multiple passages and quantitative analysis of tumor cell migration. These attributes make these AIE-active, low cytotoxic, strongly fluorescent and photostable silica nanoparticles promising for an array of biomedical applications.

Experimental section

Materials

Tetraethoxysilane (TEOS), (3-aminopropyl)triethoxysilane (APS), dimethylsulfoxide (DMSO), 1,3-dicyclohexylcarbodiimide (DCC), 4-(dimethylamino)pyridine (DMAP), biotin and other reagents were all purchased from Aldrich and used as received. Silole–APS adduct **1** was prepared according to the reported experimental procedures.[14] Human cervical cancer HeLa cells, human hepatoma BEL-7402 cells, normal liver LO2 cells and mouse fibroblast NIH 3T3 cells were purchased from Cell Resource Center, Shanghai Institutes for Biological Sciences, Chinese Academy of Sciences (China). Culture medium and fetal bovine serum (FBS) were purchased from Hyclone Labs (Logan, USA). A WST cell counting kit was purchased from Dojindo Laboratories Co (Kumamoto, Japan). Penicillin–streptomycin mixture, trypan blue exclusion assay kit, trypsin and crystal violet were bought from Sigma-Aldrich (Saint Louis, USA). An Annexin V-FITC Apoptosis Detection Kit was obtained from KeyGEN BioTECH (Nanjing, China). 2,7-Dichlorohydrofluorescein diacetate (DCFH-DA) and hematoxylin and eosin (HE) staining assay kit were obtained from Beyotime Institute of Biotechnology (Jiangsu, China).

Preparation of FSNP-1-biotin

A silole–APS conjugate (**1**) was synthesized by stirring a mixture of 6 μmol of 1,1-dimethyl-2,5-bis[4-(2-bromoethoxy)phenyl]-3,4-diphenylsilole (**2**) and 16 μmol of APS in 50 mL of DMSO overnight according to the procedure published in our previous paper.[15] Then, FSNP-**1** was fabricated by a two step sol–gel reaction.[14] Briefly, **1** was added to a mixture of ethanol (64 mL), ammonium hydroxide (1.28 mL) and distilled water (7.8 mL). The solution was then stirred at room temperature for 1 h to prepare the silole–silica nanocores, after which a mixture of 2 mL TEOS and 8 mL ethanol was slowly added. The reaction mixture was stirred at room temperature for 3 h to coat the nanocores with silica shells. FSNP-**1**-NH_2 was prepared by stirring a mixture of FSNP-**1** and APS at room temperature for additional 24 h. The nanoparticles were centrifuged and washed with ethanol and water. Finally, the FSNP-**1**-biotin was fabricated by stirring a mixture of FSNP-**1**-NH_2 and biotin at room temperature overnight in the presence of DCC and DMAP. The nanoparticles were washed with deionized water and ethanol to get rid of unwanted substances and dispersed in deionized water or ethanol for further experiments.

Characterization

The IR spectra were recorded on a Perkin-Elmer 16 PC FT-IR spectrophotometer. The chemical compositions of the nanoparticles were determined by XPS and EDX analyses. Their morphologies and sizes were investigated using JOEL 2010 TEM and JOEL 6700F SEM (JEOL Ltd Tokyo, Japan) at accelerating voltages of 200 and 5 kV, respectively. Samples were prepared by drop-casting a dilute suspension of the nanoparticles onto copper 400-mesh carrier grids covered with carbon-coated formvar films and the solvent was evaporated at room temperature in open air. The elementary particle size was estimated by measuring the diameter of 100 particles. The bioconjugation of biotin on FSNP-**1**-NH_2 was investigated by thermogravimetric analysis (TGA). PL spectra were recorded on a Perkin-Elmer LS 50B spectrofluorometer (Perkin-Elmer Corporation, USA) with Xenon discharge lamp excitation.

Cell culture

HeLa cells were cultured in minimum essential medium. BEL-7402 cells, LO2 cells and NIH 3T3 cells were grown in an RPMI 1640 medium supplemented with 10% FBS, 100 U mL^{-1} penicillin G and 100 μg mL^{-1} streptomycin in a 5% CO_2, 90% relative humidity incubator at 37 °C. Suspensions of the nanoparticles were dispersed in 0.01 M phosphate buffer solution (PBS) by an ultrasonic bath Model SB5200 (Shanghai Branson, China), diluted to various working concentrations, and then added to cells immediately. Every experiment was performed in triplicate.

Hematoxylin and eosin (HE) staining

The morphology change of cells incubated with FSNP-**1**-biotin was investigated by HE staining. The HeLa cells and 3T3 cells were seeded into a 12-well plate overnight, incubated with nanoparticles at a concentration of 0, 40 or 80 μg mL^{-1} for 48 h, fixed with 4% paraformaldehyde and then stained with hematoxylin and eosin. Hematoxylin mainly stains the chromatin in nucleus and ribosome in cytoplasm into blue and eosin mainly stains components in cytoplasm into pink or red. The cellular morphology change was observed under an Olympus CKX41 phase contrast microscope (Olympus, Japan).

Cell viability assay

The viability of cells treated with FSNP-**1**-biotin was measured using a WST-8 cell counting kit (CCK-8) according to the supplier's instruction. Cells were seeded into a 96-well plate at a density of 8000 cells per well and exposed to various concentrations of nanoparticles for 48 h. 10 μL of a CCK-8 solution was added into each well and the cells were incubated for additional 2 h at 37 °C. The optical density was measured on a microplate reader (Thermo, USA) using a test wavelength of 490 nm and a reference wavelength of 630 nm.

Trypan blue exclusion assay

To further verify the cell survival rate, a trypan blue exclusion assay was performed. The viable cells exclude trypan blue dye and are not stained to identify living cells. After being exposed to the nanoparticles for 48 h, the cells were harvested and scored as alive or dead using trypan blue according to the manufacturer's instruction. The number of viable cells was counted using a conventional hemocytometer. The rate of viability was derived by comparing with the negative control.

Annexin V-FITC/PI apoptosis assay

The quantification of apoptosis induced by FSNP-**1**-biotin in HeLa cells and 3T3 cells was analyzed by flow cytometry (FCM)

with an Annexin V-FITC/PI double staining assay. Briefly, after incubation with various concentrations of nanoparticles for 48 h, the cells were harvested with an EDTA-free trypsin solution and then treated with 5 μL Annexin V-FITC and 5 μL PI for at least 10 min at room temperature in the dark. Immediate analysis was performed using FCM (BD Biosciences, USA). For each sample, 1×10^4 cells were measured.

Intracellular reactive oxygen species assay

Detection of intracellular reactive oxygen species (ROS) was based on the peroxide-dependent oxidation of DCFH-DA to form a fluorescent compound named dichlorofluorescein (DCF). After treatment with various concentrations of FSNP-**1**-biotin or in the absence of nanoparticles as a negative control for 24 h, the cells were washed three times with PBS and incubated with 10 μM DCFH-DA at 37 °C for 20 min. The cells incubated with 50 mg L^{-1} of a Rosup solution for 30 min were treated as the positive control. The fluorescence of the cells was immediately measured using FCM (BD Biosciences, USA). For each sample, 1×10^4 cells were collected. The visual image of the ROS generation in cells was taken on an Olympus BX41 inverted fluorescence microscope (Olympus, Japan) at an excitation wavelength of 488 nm and an emission wavelength of 525 nm.

Tumor cell targeting

HeLa, BEL-7402 and LO2 cells were seeded on a round cover slip mounted onto a 6-well plate overnight. The living cells were incubated with a serum-free medium containing FSNP-**1**-biotin at a specific concentration (40 μg mL^{-1}) with or without 10 μg mL^{-1} of a biotin solution for 3 h. The cells were then washed three times with 0.01 M PBS and imaged under a Nikon A1 confocal laser scanning microscope (CLSM, Nikon Corporation, Japan) at an excitation wavelength of 405 nm.

Cellular uptake of FSNP-1-biotin

The cellular uptake and distribution of FSNP-**1**-biotin in cells were analyzed by TEM (FEI Corporation, Netherlands) according to a modified procedure.[28] Briefly, HeLa cells were treated with 40 μg mL^{-1} of FSNP-**1**-biotin for 12 h. Afterwards, the cells were washed three times with 0.01 M PBS to get rid of the unbound nanoparticles and fixed with 2.5% glutaraldehyde buffered in 0.01 M PBS for 1 h at room temperature. Fixed cells were washed three times with 0.01 M PBS and collected in a centrifuge tube, and then post-fixed in 1% osmium tetroxide for 1 h at room temperature. The sample was dehydrated by ethanol solutions at different concentrations (40, 50, 70, 80, 90, 95 and 100%), treated with propylene oxide and then embedded in Spurr's resin by infiltration with a series of mixtures of resin and propylene oxide (ratios of propylene oxide to resin: 1 : 1, 1 : 2 and 1 : 3). The resin blocks were hardened at 70 °C overnight. Ultrathin sections with a dimension of 70 nm were cut using glass knives and then stained with uranyl acetate and lead citrate prior to analysis under Tecnai G2 20 TEM (FEI Corporation, Netherlands) operating at 200 kV.

Tumor cell migration

The HeLa cells labelled with FSNP-**1**-biotin were utilized for the cell migration assay. Briefly, the cells were incubated with 40 μg mL^{-1} FSNP-**1**-biotin for 24 h, after which they were harvested, washed twice with 0.01 M PBS and resuspended in a serum-free medium at a density of 5×10^5 mL^{-1}. After addition of 600 μL culture medium with 20% or 5% serum to each well of the 24-well plate, 200 μL of the cell suspension was seeded into a millicell (8 μm pores). The cells were incubated for 24 h at 37 °C and 5% CO_2. Subsequently, the cell culture inserts were transferred into a fresh 24-well plate containing 500 μL of a pre-warmed trypsin–EDTA solution per well for 10 min at 37 °C. 100 μL of the trypsin–EDTA solution was then loaded into the quartz cell and the fluorescence from the solution at 490 nm was measured using a Perkin-Elmer LS55 spectrofluorometer (Perkin-Elmer Corporation, USA) at an excitation wavelength of 370 nm. The conventional method was performed according to the supplier's instruction with modification. Similarly, 200 μL of the cell suspension without pre-treatment with FSNP-**1**-biotin at a density of 5×10^5 mL^{-1} was seeded into a millicell. The cells were induced to migrate by the serum medium in the lower compartment. After removal of non-migrated cells in the upper compartment, the cells were stained with 0.1% crystal violet and observed under an optical microscope (Olympus, Japan).

Statistical analysis

Data are expressed as mean ± standard deviation. Statistical analysis was performed using one-way analysis of variance (ANOVA) with PASW Statistics 18.0 (Chicago, USA). The level of significance for all the comparisons was $P < 0.05$.

Acknowledgements

The authors thank the support from the Programs for Science and Technology Development of Wuhan City, Hubei Province (201260523172-8), the Research Project Competition of HKUST (RPC11SC09 and RPC10SC13), the Research Grants Council of Hong Kong (604711, 603509, HKUST2/CRF/10 and N_HKUST620/11), the National Science Foundation of China (20974028), the Innovation and Technology Commission (ITCPP/17-9), and the University Grants Committee of Hong Kong (AoE/P-03/08).

References

1 (*a*) L. Wang, K. M. Wang, S. Santra, X. J. Zhao, L. R. Hilliard, J. E. Smith, J. R. Wu and W. H. Tan, *Anal. Chem.*, 2006, **78**, 646–654; (*b*) S. Santra, *Methods Mol. Biol.*, 2010, **624**, 151–162.
2 X. Zhou and J. Zhou, *Anal. Chem.*, 2004, **76**, 5302–5312.
3 W. Lian, S. A. Litherland, H. Badrane, W. Tan, D. Wu, H. V. Baker, P. A. Gulig, D. V. Lim and S. Jin, *Anal. Biochem.*, 2004, **334**, 135–144.
4 L. M. Rossi, L. Shi, F. H. Quina and Z. Rosenzweig, *Langmuir*, 2005, **21**, 4277–4280.
5 S. Santra, H. Yang, D. Dutta, J. T. Stanley, P. H. Holloway, W. Tan, B. M. Moudgil and R. A. Mericle, *Chem. Commun.*, 2004, 2810–2811.

6 I. Sokolov and S. Naik, *Small*, 2008, **4**, 934–939.
7 (*a*) J. M. Rosenholm, A. Meinander, E. Peuhu, R. Niemi, J. E. Eriksson, C. Sahlgren and M. Linden, *ACS Nano*, 2009, **3**, 197–206; (*b*) X. Le Guevel, B. Hotzer, G. Jung and M. Schneider, *J. Mater. Chem.*, 2011, **21**, 2974–2981; (*c*) C. P. Tsai, C. Y. Chen, Y. Hung, F. H. Chang and C. Y. Mou, *J. Mater. Chem.*, 2009, **19**, 5737–5743.
8 (*a*) Y. Jin, S. Kannan, M. Wu and J. X. Zhao, *Chem. Res. Toxicol.*, 2007, **20**, 1126–1133; (*b*) E. J. Park and K. Park, *Toxicol. Lett.*, 2009, **184**, 18–25.
9 H. Ow, D. R. Larson, M. Srivastava, B. A. Baird, W. W. Webb and U. Wiesner, *Nano Lett.*, 2005, **5**, 113–117.
10 (*a*) Y. Hong, J. W. Y. Lam and B. Z. Tang, *Chem. Commun.*, 2009, 4332–4353; (*b*) Y. Hong, J. W. Y. Lam and B. Z. Tang, *Chem. Soc. Rev.*, 2011, **40**, 5361–5388.
11 X. Michalet, F. F. Pinaud, L. A. Bentolila, J. M. Tsay, S. Doose, J. J. Li, G. Sundaresan, A. M. Wu, S. S. Gambhir and S. Weiss, *Science*, 2005, **307**, 538–544.
12 (*a*) J. Luo, Z. Xie, J. W. Y. Lam, L. Cheng, H. Chen, C. Qiu, H. S. Kwok, X. Zhan, Y. Liu, D. Zhu and B. Z. Tang, *Chem. Commun.*, 2001, 1740–1741; (*b*) Q. L. Zhao, K. Li, S. J. Chen, A. J. Qin, D. Ding, S. Zhang, Y. Liu, B. Liu, J. Z. Sun and B. Tang, *J. Mater. Chem.*, 2012, **22**, 15128–15135.
13 Z. Li, Y. Dong, B. Mi, Y. Tang, M. Haussler, H. Tong, J. W. Y. Lam, Y. Ren, H. H. Sung, K. S. Wong, P. Gao, I. D. Williams, H. S. Kwok and B. Z. Tang, *J. Phys. Chem. B*, 2005, **109**, 10061–10066.
14 M. Faisal, Y. Hong, J. Liu, Y. Yu, J. W. Y. Lam, A. Qin, P. Lu and B. Z. Tang, *Chem.–Eur. J.*, 2010, **16**, 4266–4272.
15 F. Mahtab, Y. Yu, J. W. Y. Lam, J. Z. Liu, B. Zhang, P. Lu, X. X. Zhang and B. Z. Tang, *Adv. Funct. Mater.*, 2011, **21**, 1733–1740.
16 (*a*) K. Y. Pu and B. Liu, *Adv. Funct. Mater.*, 2011, **21**, 3408–3423; (*b*) F. M. Kievit and M. Zhang, *Adv. Mater.*, 2011, **23**, H217–H247; (*c*) T. M. Allen, *Nat. Rev. Cancer*, 2002, **2**, 750–763; (*d*) C. H. Lai, C. Y. Lin, H. T. Wu, H. S. Chan, Y. J. Chuang, C. T. Chen and C. C. Lin, *Adv. Funct. Mater.*, 2010, **20**, 3948–3958.
17 (*a*) K. Na, T. Bum Lee, K. H. Park, E. K. Shin, Y. B. Lee and H. K. Choi, *Eur. J. Pharm. Sci.*, 2003, **18**, 165–173; (*b*) W. Yang, Y. Cheng, T. Xu, X. Wang and L. P. Wen, *Eur. J. Med. Chem.*, 2009, **44**, 862–868; (*c*) S. Chen, X. Zhao, J. Chen, L. Kuznetsova, S. S. Wong and I. Ojima, *Bioconjugate Chem.*, 2010, **21**, 979–987; (*d*) D. N. Heo, D. H. Yang, H. J. Moon, J. B. Lee, M. S. Bae, S. C. Lee, W. J. Lee, I. C. Sun and I. K. Kwon, *Biomaterials*, 2012, **33**, 856–866.
18 Y. B. Patil, S. K. Swaminathan, T. Sadhukha, L. Ma and J. Panyam, *Biomaterials*, 2010, **31**, 358–365.
19 Z. Zhao, Z. Wang, P. Lu, C. Y. Chan, D. Liu, J. W. Y. Lam, H. H. Sung, I. D. Williams, Y. Ma and B. Z. Tang, *Angew. Chem., Int. Ed.*, 2009, **48**, 7608–7611.
20 L. Sun, Y. Li, X. Liu, M. Jin, L. Zhang, Z. Du, C. Guo, P. Huang and Z. Sun, *Toxicol. In Vitro*, 2011, **25**, 1619–1629.
21 (*a*) E. J. Park, J. Yi, K. H. Chung, D. Y. Ryu, J. Choi and K. Park, *Toxicol. Lett.*, 2008, **180**, 222–229; (*b*) M. Ahamed, R. Posgai, T. J. Gorey, M. Nielsen, S. M. Hussain and J. J. Rowe, *Toxicol. Appl. Pharmacol.*, 2010, **242**, 263–269.
22 C. F. Jones and D. W. Grainger, *Adv. Drug Delivery Rev.*, 2009, **61**, 438–456.
23 M. Mahmoudi, K. Azadmanesh, M. A. Shokrgozar, W. S. Journeay and S. Laurent, *Chem. Rev.*, 2011, **111**, 3407–3432.
24 M. D. Chavanpatil, A. Khdair and J. Panyam, *J. Nanosci. Nanotechnol.*, 2006, **6**, 2651–2663.
25 Z. Chu, Y. Huang, Q. Tao and Q. Li, *Nanoscale*, 2011, **3**, 3291–3299.
26 Y. Yu, C. Feng, Y. N. Hong, J. Z. Liu, S. J. Chen, K. M. Ng, K. Q. Luo and B. Z. Tang, *Adv. Mater.*, 2011, **23**, 3298–3302.
27 J. Condeelis and J. W. Pollard, *Cell*, 2006, **124**, 263–266.
28 A. Nan, X. Bai, S. J. Son, S. B. Lee and H. Ghandehari, *Nano Lett.*, 2008, **8**, 2150–2154.

